Portable spherical array probe for volumetric real-time optoacoustic imaging at centimeter-scale depths

X. Luís Deán-Ben[1] and Daniel Razansky[1,2,*]

[1]*Institute for Biological and Medical Imaging (IBMI), Helmholtz Center Munich, Ingolstädter Landstraße 1, 85764 Neuherberg, Germany*

[2]*Faculty of Medicine, Technical University of Munich, Ismaninger Straße 22, 81675 Munich, Germany*

**dr@tum.de*

Abstract: We report on a novel hand-held imaging probe for real-time optoacoustic visualization of deep tissues in three dimensions. The system incorporates an annular two-dimensional array of ultrasonic sensors densely distributed on a spherical surface. Simultaneous recording and processing of time-resolved data from all the channels enables acquisition of entire volumetric data sets for each illumination laser pulse. The proposed solution utilizes a transparent membrane in order to allow efficient coupling of optoacoustically generated waves to the ultrasonic detectors while avoiding direct contact of the imaged object with the coupling medium. The hand-held approach further allows convenient handling of both pre-clinical experiments as well as clinical measurements in human subjects. Here we demonstrate an imaging speed of 10 volumetric frames per second with spatial resolution down to 200 micrometers in the imaged region while also achieving imaging depth of more than 1.5 cm in living tissues without signal averaging.

OCIS codes: (170.3880) Medical and biological imaging; (110.5120) Photoacoustic imaging; (110.6955) Tomographic imaging.

References and links

1. D. Razansky, N. C. Deliolanis, C. Vinegoni, and V. Ntziachristos, "Deep tissue optical and optoacoustic molecular imaging technologies for pre-clinical research and drug discovery," Curr. Pharm. Biotechnol. **13**(4), 504–522 (2012).
2. M. A. Pysz, S. S. Gambhir, and J. K. Willmann, "Molecular imaging: current status and emerging strategies," Clin. Radiol. **65**(7), 500–516 (2010).
3. F. Leblond, S. C. Davis, P. A. Valdés, and B. W. Pogue, "Pre-clinical whole-body fluorescence imaging: Review of instruments, methods and applications," J. Photochem. Photobiol. B **98**(1), 77–94 (2010).
4. C. Vinegoni, C. Pitsouli, D. Razansky, N. Perrimon, and V. Ntziachristos, "In vivo imaging of Drosophila melanogaster pupae with mesoscopic fluorescence tomography," Nat. Methods **5**(1), 45–47 (2007).
5. L. V. Wang and H.-I. Wu, *Biomedical optics: principles and imaging* (Wiley, 2007).
6. L. V. Wang and S. Hu, "Photoacoustic tomography: in vivo imaging from organelles to organs," Science **335**(6075), 1458–1462 (2012).
7. P. Beard, "Biomedical photoacoustic imaging," Interface Focus **1**(4), 602–631 (2011).
8. D. Razansky, "Multi-spectral optoacoustic tomography – volumetric color hearing in real time," IEEE J. Sel. Top. Quantum Electron. **18**(3), 1234–1243 (2012).
9. E. Herzog, A. Taruttis, N. Beziere, A. A. Lutich, D. Razansky, and V. Ntziachristos, "Optical imaging of cancer heterogeneity with multispectral optoacoustic tomography," Radiology **263**(2), 461–468 (2012).
10. J. J. Yao, J. Xia, K. I. Maslov, M. Nasiriavanaki, V. Tsytsarev, A. V. Demchenko, and L. V. Wang, "Noninvasive photoacoustic computed tomography of mouse brain metabolism in vivo," Neuroimage **64**, 257–266 (2013).
11. L. Tong, Q. S. Wei, A. Wei, and J. X. Cheng, "Gold nanorods as contrast agents for biological imaging: optical properties, surface conjugation and photothermal effects," Photochem. Photobiol. **85**(1), 21–32 (2009).
12. A. Buehler, E. Herzog, A. Ale, B. A. Smith, V. Ntziachristos, and D. Razansky, "High resolution targeting of tumor apoptosis in living mice by means of multispectral optoacoustic tomography," Eur. J. Nucl. Med. Mol. Imag. Res. **2**, 14 (2012).
13. J. Laufer, P. Johnson, E. Zhang, B. Treeby, B. Cox, B. Pedley, and P. Beard, "In vivo preclinical photoacoustic imaging of tumor vasculature development and therapy," J. Biomed. Opt. **17**(5), 056016 (2012).

14. S. P. Johnson, J. G. Laufer, E. Z. Zhang, P. C. Beard, and R. B. Pedley, "Determination of differential tumour vascular pathophysiology in vivo by photoacoustic imaging," Eur. J. Cancer **48**, S186–S187 (2012).
15. R. Ma, M. Distel, X. L. Deán-Ben, V. Ntziachristos, and D. Razansky, "Non-invasive whole-body imaging of adult zebrafish with optoacoustic tomography," Phys. Med. Biol. **57**(22), 7227–7237 (2012).
16. B. Xia, D. Piras, J. C. G. van Hespen, W. Steenbergen, and S. Manohar, "A new acoustic lens material for large area detectors in photoacoustic breast tomography," Photoacoustics **1**(2), 9–18 (2013).
17. J. M. Yang, C. Favazza, R. Chen, J. Yao, X. Cai, K. Maslov, Q. Zhou, K. K. Shung, and L. V. Wang, "Simultaneous functional photoacoustic and ultrasonic endoscopy of internal organs in vivo," Nat. Med. **18**(8), 1297–1302 (2012).
18. D. Razansky, N. J. Harlaar, J. L. Hillebrands, A. Taruttis, E. Herzog, C. J. Zeebregts, G. M. van Dam, and V. Ntziachristos, "Multispectral optoacoustic tomography of matrix metalloproteinase activity in vulnerable human carotid plaques," Mol. Imaging Biol. **14**(3), 277–285 (2012).
19. Y. Xu, L. V. Wang, G. Ambartsoumian, and P. Kuchment, "Reconstructions in limited-view thermoacoustic tomography," Med. Phys. **31**(4), 724–733 (2004).
20. R. A. Kruger, R. B. Lam, D. R. Reinecke, S. P. Del Rio, and R. P. Doyle, "Photoacoustic angiography of the breast," Med. Phys. **37**(11), 6096–6100 (2010).
21. D. Van de Sompel, L. S. Sasportas, A. Dragulescu-Andrasi, S. Bohndiek, and S. S. Gambhir, "Improving image quality by accounting for changes in water temperature during a photoacoustic tomography scan," PLoS ONE **7**(10), e45337 (2012).
22. H. P. Brecht, R. Su, M. Fronheiser, S. A. Ermilov, A. Conjusteau, and A. A. Oraevsky, "Whole-body three-dimensional optoacoustic tomography system for small animals," J. Biomed. Opt. **14**(6), 064007 (2009).
23. D. R. Reinecke, R. A. Kruger, R. B. Lam, and S. P. Del Rio, "Co-registered photoacoustic, thermoacoustic and ultrasound mouse imaging," Proc. SPIE **7564**, 756420, 756420-9 (2010).
24. A. Buehler, X. L. Deán-Ben, J. Claussen, V. Ntziachristos, and D. Razansky, "Three-dimensional optoacoustic tomography at video rate," Opt. Express **20**(20), 22712–22719 (2012).
25. M. P. Fronheiser, S. A. Ermilov, H. P. Brecht, A. Conjusteau, R. Su, K. Mehta, and A. A. Oraevsky, "Real-time optoacoustic monitoring and three-dimensional mapping of a human arm vasculature," J. Biomed. Opt. **15**(2), 021305 (2010).
26. C. Kim, T. N. Erpelding, L. Jankovic, M. D. Pashley, and L. V. Wang, "Deeply penetrating in vivo photoacoustic imaging using a clinical ultrasound array system," Biomed. Opt. Express **1**(1), 278–284 (2010).
27. P. D. Kumavor, C. Xu, A. Aguirre, J. Gamelin, Y. Ardeshirpour, B. Tavakoli, S. Zanganeh, U. Alqasemi, Y. Yang, and Q. Zhu, "Target detection and quantification using a hybrid hand-held diffuse optical tomography and photoacoustic tomography system," J. Biomed. Opt. **16**(4), 046010 (2011).
28. D. Queiros, X. L. Dean-Ben, A. Buehler, D. Razansky, A. Rosenthal, and V. Ntziachristos, "Modeling the shape of cylindrically focused transducers in three-dimensional optoacoustic tomography," J. Biomed. Opt. **18**(7) 076014 (2013).
29. A. Taruttis, M. Wildgruber, K. Kosanke, N. Beziere, K. Licha, R. Haag, M. Aichler, A. Walch, E. Rummeny, and V. Ntziachristos, "Multispectral optoacoustic tomography of myocardial infarction," Photoacoustics **1**(1), 3–8 (2013).
30. X. L. Deán-Ben, A. Buehler, V. Ntziachristos, and D. Razansky, "Accurate model-based reconstruction algorithm for three-dimensional optoacoustic tomography," IEEE Trans. Med. Imaging **31**(10), 1922–1928 (2012).
31. A. Rosenthal, V. Ntziachristos, and D. Razansky, "Model-based optoacoustic inversion with arbitrary-shape detectors," Med. Phys. **38**(7), 4285–4295 (2011).
32. X. L. Deán-Ben, D. Razansky, and V. Ntziachristos, "The effects of acoustic attenuation in optoacoustic signals," Phys. Med. Biol. **56**(18), 6129–6148 (2011).
33. A. Rosenthal, V. Ntziachristos, and D. Razansky, "Optoacoustic methods for frequency calibration of ultrasonic sensors," IEEE Trans. Ultrason. Ferroelectr. Freq. Control **58**(2), 316–326 (2011).
34. X. L. Deán-Ben, V. Ntziachristos, and D. Razansky, "Artefact reduction in optoacoustic tomographic imaging by estimating the distribution of acoustic scatterers," J. Biomed. Opt. **17**(11), 110504 (2012).

1. Introduction

Optical imaging has proven to be the most versatile tool for probing function at the cellular and molecular level, mainly due to the highly specific contrast provided by interaction of photons with tissues [1–3]. The main limitation of the optical spectrum is light diffusion, which strongly limits the achievable resolution at depths beyond several hundred microns [4]. Thereby, the resolution of optical techniques in deep tissues typically scales as ~1/10 of the imaging depth [5]. Such resolution limitation can be efficiently overcome by means of optoacoustic excitation, which utilizes absorption of short-pulsed optical illumination in order to generate ultrasonic responses. In this way, optoacoustic techniques are able to achieve spatial resolution in the range of 1/200 of the imaging depth [6], resulting in a unique combination of rich contrast provided by excitation at optical wavelengths and high resolution imaging performance deep in scattering tissues [7,8]. By combining illumination at multiple wavelengths, multispectral optoacoustic tomography (MSOT) is further able to spectrally

identify functional parameters, such as blood oxygenation [9,10], as well as track distribution of extrinsically-administered molecular contrast agents targeted to specific disease hallmarks [11,12]. To this end, optoacoustics has indeed defined several important new application areas in small animal research [10,13–15] and is currently explored for selected clinical imaging applications [16–18].

Yet, the currently available optoacoustic systems are not suitable for fast and accurate deep tissue imaging in realistic clinical scenarios using hand-held operation. In general, performance of any optoacoustic imaging system would depend upon the particular arrangement of the illumination and ultrasonic detection setups, so that the advantages and disadvantages for a certain application are determined by the shaping of the illumination beam as well as the number, type, detection area and scanning positions of the ultrasonic detectors employed. It has been long recognized that the most efficient implementation of optoacoustic imaging implies simultaneous collection of time-resolved optoacoustic signals in three dimensions from as many locations (projections) around the imaged object as possible, thus avoiding limited-view effects [19]. Thereby, attempts to achieve high fidelity imaging were based on rotating (scanning) a set of transducers around a stationary object so that signals at a large number of locations are acquired for optimal tomographic reconstruction [20]. Since the acquired optoacoustic responses are generally low, scanning-based optoacoustic imaging systems have resulted in prolonged acquisition times [21–23], hindering hand-held operation and imaging of fast dynamic processes. In addition, motion artifacts in the imaged object during the scanning procedure due to e.g. breathing, heart beating and other factors would further deteriorate spatial resolution and quantitativeness of the retrieved images. More recent volumetric optoacoustic imaging approach employed no scanning [24], however, was also not intended for hand-held use.

Alternatively, hand-held optoacoustic imaging probes have been proposed based on incorporating an illumination set-up into the standard ultrasonic linear arrays [25–27]. Due to the linear array geometry, the images retrieved with such probes correspond to cross-sections along the depth direction. Such arrangement however may not be suitable to clearly identify long structures distributing in parallel to the object's surface (skin), such as vasculature. Furthermore, reconstruction is done by assuming that all signals are generated in the imaging plane. Such inaccurate hypothesis generally results in creation of out-of-plane artefacts [28] as well as anisotropic resolution if a large volume is imaged by scanning. These reconstruction inaccuracies may consequently severely affect the quantification performance, commonly required in functional and molecular imaging applications involving absolute measurement of e.g. oxygenation levels or concentrations of contrast agents [9,10,12,29]. In addition, for piezo-electric detection elements, the effective angular coverage of planar arrays is affected by the frequency-dependent sensitivity field of its individual elements. As a result, the individual elements mainly detect waves excited along the normal to their surface, i.e. the generated optoacoustic signals are only collected from locations covering a very limited solid angle around each imaged point. Thus, the reconstructions are strongly affected by limited view effects with consequent severe deterioration of tomographic image quality and image quantification ability.

The proposed solution utilizes a hand-held design approach, in which a two-dimensional array of ultrasonic detectors is arranged on a spherical surface. In this way, the individual elements can most efficiently collect signals generated in the region of interest located around the centre of the sphere. Since many imaging scenarios, such as imaging of large areas of human body, do not allow full tomographic access to the imaged area from all directions, this particular arrangement is particularly advantageous for optoacoustic imaging as the generated signals are optimally collected from as broad as possible range of angles (projections) around the imaged area located inside the living subject. Here we assess the basic imaging performance metrics of the newly introduced probe design and evaluate its capacity for dynamic (real-time) three-dimensional visualization at depths in the order of centimeters in highly scattering and absorbing tissues.

2. Materials and methods

2.1. The deep tissue imaging probe

The geometry of the custom-made three-dimensional imaging probe (Imasonic SaS, Voray, France) is depicted in Figs. 1(a)-1(b) with its actual photograph shown in Fig. 1(f). The transducer array consists of 256 ultrasonic elements, manufactured using piezocomposite technology and disposed on a spherical surface covering an angle of 90º (solid angle of $2\pi[1-\cos(\pi/4)]$) as shown in Fig. 1(a). The active detection aperture includes a circular opening in the centre with a diameter of 8 mm for optical illumination. Figure 1(c) showcases the frequency response of the individual array elements having a central frequency of 4 MHz and a full-width at half maximum (FWHM) of 100%. All the elements have an approximate size of 3x3 mm^2 (Fig. 1(b)) while their normal is oriented towards the centre of the sphere, thereby also providing good sensitivity for all detection elements in the region of interest (ROI) located around centre of the sphere. Since the sensitivity of the individual elements is space- and frequency-dependent, it is thus also conditioned by the size and shape of the optoacoustic sources. Considering that the acoustic pressure is integrated on the active surface of the transducer elements, the sensitivity field $S(r')$ (in modulus) of an element for a given frequency f can be estimated by considering a monochromatic acoustic wave as

$$S(r') = \mathrm{mod}\{\int_r \exp(ik\,|\,r'-r\,|)dr\} \approx \mathrm{mod}\{\sum_j \exp(ik\,|\,r'-r_j\,|)\Delta r_j\}, \qquad (1)$$

where $k=2\pi f/c$ is the wavenumber, c is the speed of sound in the medium and Δr_j the area associated to position r_j on the active surface of the transducer. Figure 1(d) shows the combined sensitivity field calculated as superposition of the sensitivity fields for all the elements at three different frequencies within the available detection bandwidth. Considering that optoacoustic reconstruction is generally based on integrating contributions from all the sensors (as for instance is done in back-projection algorithms), the combined sensitivity field establishes an estimate of the size of the effective imaging region. Figure 1(e) displays the FWHM values of the size of the combined sensitivity field at various ultrasonic frequencies. Naturally, the effective imaging region can be expanded by reducing the size of the individual detection elements. However, relatively large elements are generally required to provide an acceptable signal-to-noise ratio (SNR) for dynamic hand-held deep tissue imaging, for which no signal averaging can be applied for noise suppression.

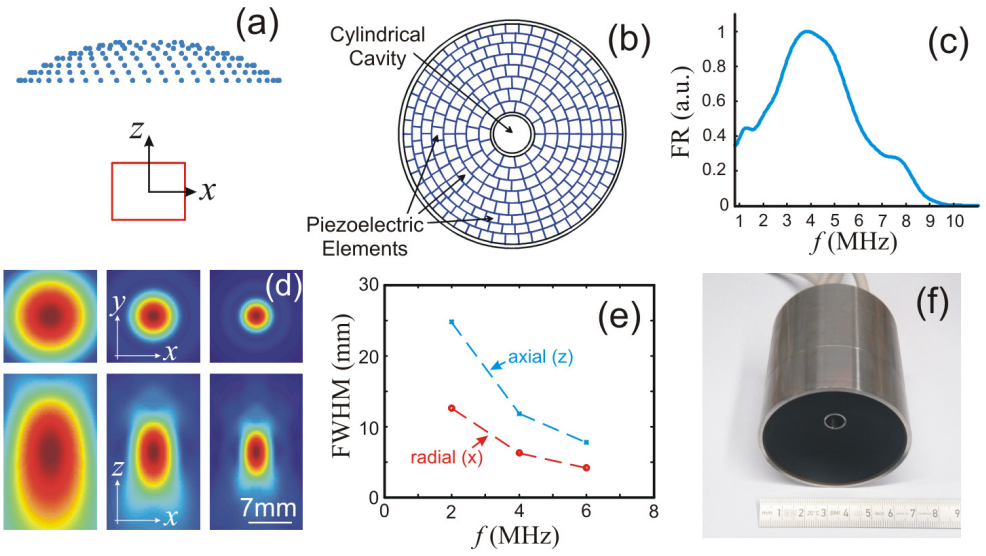

Fig. 1. The portable spherical array probe for volumetric real-time optoacoustic imaging. (a) Side view of the location of the transducer elements (blue points) and the corresponding effective imaging region of the array (red square). (b) Top-view showing the shape of the individual piezoelectric detection elements. (c) Frequency response of the individual elements for a point source located in the centre of the spherical surface. (d) Combined sensitivity field for three different acoustic frequencies. (e) Dimensions of the effective imaging region as a function of the frequency emitted by the optical absorbers. (f) Photograph of the probe.

The size and orientation of the ultrasound transducer array also affect the achievable resolution and overall quality of the retrieved images. Figure 2(a) shows a simulated example of reconstructions obtained for a certain distribution of optical absorbers. Each absorber corresponded to a three-dimensional truncated parabolic distribution with 200 μm diameter, for which the optoacoustic signals can be calculated analytically [28]. Three different scenarios were taken into account for the reconstruction, which was done with a model-based inversion algorithm [30]. In the first case, the analytical pressure signals for the central positions of the array elements were considered. Secondly, the same signals were taken but after convolving them with the electrical impulse response of the detectors. Finally, the reconstruction was done using the averaged pressure signals on the surface of the elements. The results of the reconstructions for these three cases are showcased in Figs. 2(b)-2(d) respectively, from which it becomes clear that certain image distortions are produced even when using ideal analytical signal shapes. This is due to the limited angular coverage of the array, which is considered inevitable when imaging large volumes with the imaging region only accessible from one side, as it usually occurs in the case of hand-held human imaging. Nevertheless, the effective angular coverage is in fact maximized with the spherical distribution of elements oriented towards the imaging region, so this configuration is superior to linear or planar array arrangements with respect to limited-view image artefacts. Figures 2(c)-2(d) further showcase that the effects of the transducer response can further distort the images and negatively affect the achievable resolution, if point detectors with infinite bandwidth are assumed for the reconstructions [31]. Other acoustic propagation effects such as acoustic attenuation also reduce the attained resolution, although distortions for low frequencies mainly arise due to non-ideal transducer characteristics [32].

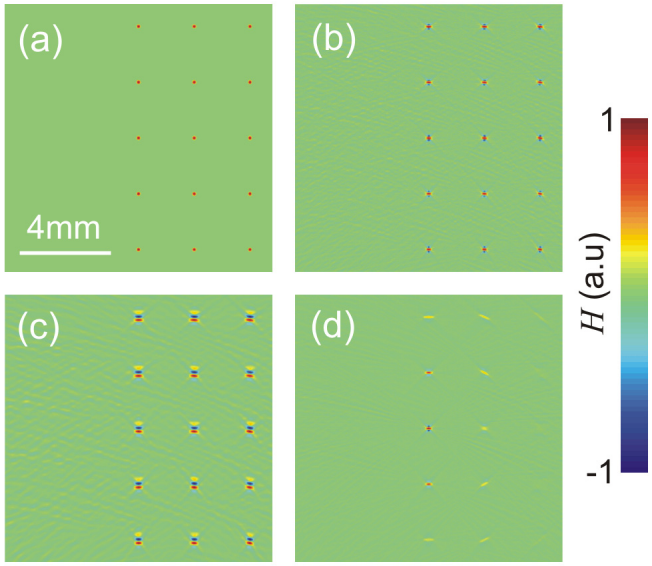

Fig. 2. Simulated optoacoustic reconstructions of parabolic optical absorbers. The images represent cross-sections in the plane y=0. (a) Theoretical distribution of the optical absorbers. (b) Reconstruction obtained by assuming point detectors. (c) Reconstruction obtained with point detectors by further convolving the detected pressure variation with the impulse response of the transducer elements. (d) Reconstruction obtained by averaging the detected pressure variations over the effective active area of the elements.

2.2. Experimental description

The optical excitation for the hand-held probe is provided via a custom-made silica fused-end fibre bundle (CeramOptics GmbH, Bonn, Germany) guided through a cylindrical cavity in the centre of the array. The individual fibres at the output end are randomly distributed with respect to the input of the fibre bundle, so that the output beam can be approximated as Gaussian with a numerical aperture of 0.22. This leads to a beam width (full-width at half maximum) of approximately 10 mm at a distance of 30 mm within water medium (refraction index 1.33), which is approximately where the surface of the tissue is located. This is consistent with the beam size and shape observed experimentally. The efficiency of light coupling through the fibre bundle is approximately 75%, mainly due to input coupling losses and reflections at the output end. A short-pulsed (<10 ns duration) wavelength-tunable (690-900 nm) optical parametric oscillator (OPO) laser (Phocus, Opotek Inc., Carlsbad, CA) with pulse repetition rate of 10 Hz is used as an optical source. The 256 optoacoustic signals are simultaneously acquired with the spherical transducer array while the signals are sampled at 40 megasamples per second using analog to digital converters. The signals are transmitted in real time to a PC workstation that performs deconvolution with electrical impulse response of the detectors [33], band-pass filtering with cut-off frequencies between 200 kHz and 7 MHz and image reconstruction using the model-based approach. For acoustic coupling, the probe is either fully immersed into a water tank or a transparent polyethylene membrane (approximately 10 μm thickness), which contains a matching fluid, is used instead for hand-held operation.

Several experiments were subsequently performed to characterize the optoacoustic probe design and evaluate its performance for real-time volumetric imaging in deep tissues. For experimental determination of resolution of the system, a polyethilene microsphere with an approximate diameter of 50 μm (Cospheric BKPMS 45-53um) was used. The sphere was then moved to approximately the same set of positions that was previously simulated in Fig. 2. The reconstruction was done with the model-based inversion algorithm [30]. The illumination wavelength was set to 750 nm corresponding to the maximum power of the laser.

Two additional experiments were done to showcase the dynamic imaging capabilities of the system. In the first one, we monitored injection of mouse blood into a polyethylene tubing with an inner diameter of 0.6 mm. The tube was placed at 15 mm depth within tissue mimicking medium that consisted of an agar matrix (1.3% agar by weight) containing 0.002% by volume of black India ink and 1.2% by volume of Intralipid to simulate a standard background absorption coefficient (μ_a=0.2 cm^{-1}) and reduced scattering coefficient (μ'_s=10 cm^{-1}) in biological tissues (Fig. 4(a)). In the second experiment, the system was used in a hand-held operation mode for imaging an arm and forearm of a healthy volunteer. In all cases, the illumination was set to 800 nm corresponding to the isosbestic point of haemoglobin.

3. Results

Results of the experimentally determined resolution of the system are displayed in Fig. 3. As a representative example, three different cross-sectional views of the images obtained for the microsphere located in the centre of the spherical surface can be seen in Figs. 3(a)-3(c) along with three one dimensional profiles normal to the cross-sectional planes. From the image reconstructed at each location of the microsphere, the resolution in x, y and z is estimated from the dimensions of a cuboid enclosing all the points with the reconstructed absorption higher than half the maximum value (after also subtracting the microsphere's diameter from the cuboids' dimensions). Figs. 3(d)-3(f) display the estimated resolution in x, y and z directions as a function of the position of the microsphere. In this way the best achievable resolution was estimated in the order of 200 μm. It is important to notice that these values correspond to propagation of the ultrasonic waves in a uniform acoustic medium (water). If acoustic heterogeneities are present, the resolution is generally reduced so that an additional algorithm might be necessary in order to at least partially recover for deterioration of the image quality [34].

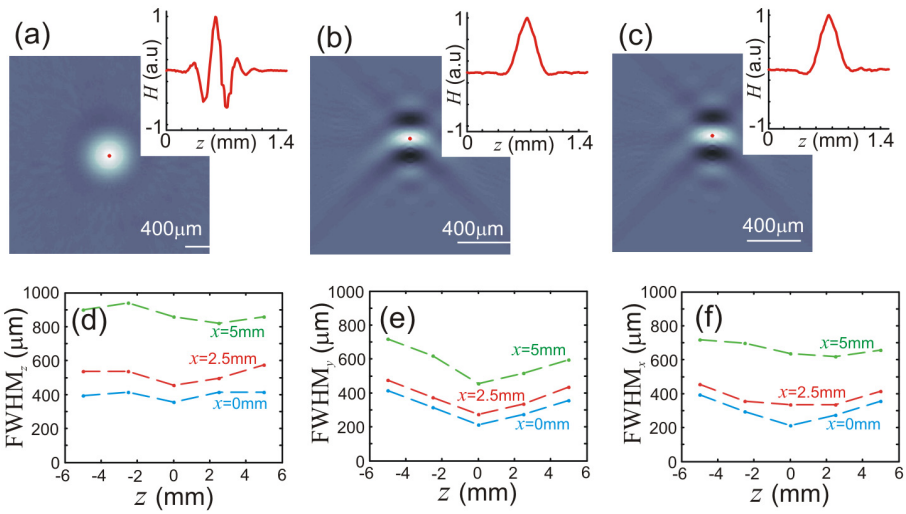

Fig. 3. Experimental determination of the spatial resolution. (a) Cross-section (normal to the z axis) from the reconstructed volumetric image of a 50 μm diameter sphere located in the centre of the sphere. (b) Cross-section normal to the y axis. (c) Cross-section normal to the x axis. The insets show the corresponding one-dimensional profiles in the direction normal to the cross-sectional planes (the position of the profiles are indicated with a red dot). The estimated resolution for the z, y and x directions are plotted in (d), (e) and (f) as a function of the position of the microsphere on the x and z axes.

Figure 4 shows the results of the blood injection experiment. In particular, the reconstructed three-dimensional transparency views for 8 different time instants are shown in

Fig. 4(b). The results clearly indicate the feasibility of real-time monitoring of dynamic events in three dimensions, e.g. for monitoring blood perfusion in deep-seated structures. The dynamic imaging performance can be best visualized in a video file available in the online version of the journal (Media 1), showing the entire sequence of frames for a duration of 35 s.

Finally, results corresponding to the hand-held human imaging experiment are displayed in Fig. 5. The volumetric images correspond to a single-shot illumination, i.e. no signal averaging was performed. The images are normalized with an exponential decay function along the *z* (depth) direction to provide first-order correction for the effects of light attenuation in deep tissues. In Fig. 5(a) the images are presented with three-dimensional transparency maps while Fig. 5(b) shows the maximum intensity projections (MIP) views along the lateral (radial) *x* direction. Due to exponential normalization versus depth, the images are increasingly afflicted with noise as the depth increases. Nevertheless, blood vessels, located at depths beyond 1.5 cm in highly scattering and absorbing muscle tissue, can be clearly identified with a good signal-to-noise ratio, showcasing the deep tissue real-time imaging capacity of the probe.

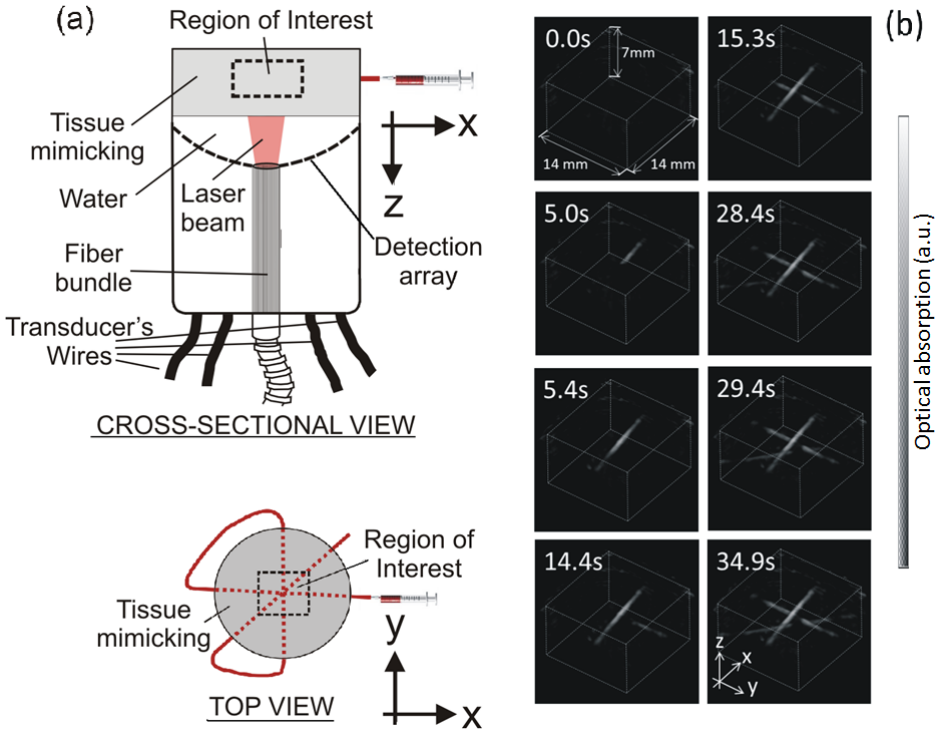

Fig. 4. Real-time monitoring of blood injection into a tube located approximately at 15 mm depth within a phantom mimicking optical and acoustic properties of soft tissues. All images were acquired with a single laser pulse without signal averaging. (a) Schematic representation of the experimental set-up. (b) Reconstructed images (represented as three-dimensional transparency views) for eight different time instants (See Media 1).

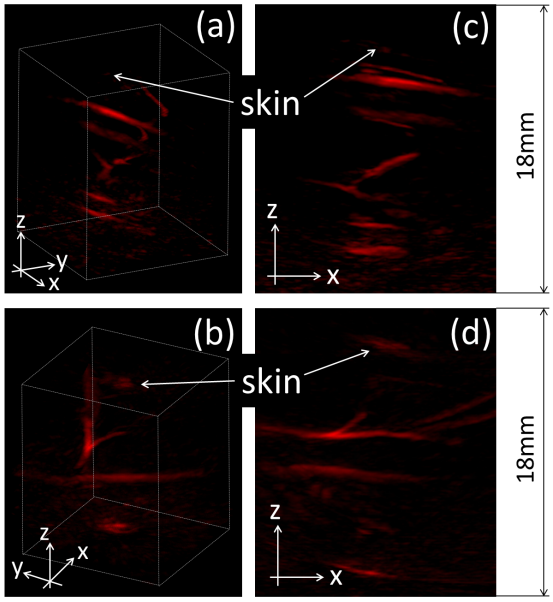

Fig. 5. Hand-held imaging experiment in a human volunteer. The images were acquired with a single laser pulse without signal averaging. (a) Three-dimensional transparency view of two different tomographic reconstructions. (b) Maximum intensity projections along the *x* direction. Vessels at a depth of more than 1.5 cm are clearly visible.

4. Discussion and conclusions

In this work, an optoacoustic probe for volumetric deep tissue imaging, has been presented and characterized. The proposed hand-held design is in fact the key aspect of the newly introduced approach as it allows convenient handling of both pre-clinical experiments as well as clinical measurements. The solution therefore uses a transparent membrane in order to allow efficient coupling of the optoacoustically-generated waves to the ultrasonic detectors while avoiding direct contact of the imaged object with the coupling medium. Yet, the hand-held arrangement imposes additional requirements. When the measurement head is held by hand and not fixed relative to the object, the images must be acquired in real-time without signal averaging (single pulse acquisition) in order to avoid motion artefacts. Herein the specific arrangement of illumination and detection elements has been optimized for high-performance hand-held operation and rendering three dimensional images in real time. In particular, maximal size and appropriate orientation of the ultrasonic transducers are essential to efficiently collect the optoacoustic signals generated in the imaging region. The three-dimensional acquisition and reconstruction approach further helps to increase the effective tomographic coverage and significantly reduce image artefacts associated with the limited-view problems, which may also assist with making the images more quantitative and identify the correct shape and size of structures within tissues.

The geometrical characteristics of the ultrasonic array employed to collect the signals are optimized for deep tissue imaging. Thereby, the piezoelectric elements are densely distributed on the surface of a sphere and oriented towards its centre. This configuration maximizes the signal-to-noise ratio for signals generated in the imaged region around the centre of the sphere, as all the elements are highly sensitive in this area. In addition, the good sensitivity of large number of elements in the imaged region maximizes the effective tomographic coverage, thus minimizing again the negative effects of limited-view reconstructions. On the other hand, the concentric illumination design also helps increasing the light intensity reaching the imaged region, in contrast to other hand-held optoacoustic probe designs in

which optical excitation is provided on the lateral sides of a linear ultrasonic array, thus most light is deposited outside the imaged plane.

Depending on the characteristic size and distribution of optical absorbers of interest, the current design supports a relatively small effective field of view on the order of 15 mm in the axial direction and 10 mm in the radial (lateral) directions. By increasing the number of detection elements and consequently decreasing their size, the field of view can be increased. However, this may lead to decreased sensitivity of the individual elements, which could eventually compromise the real-time imaging capabilities of the probe, especially in deep tissue areas.

The experimental results clearly indicate feasibility of rendering three-dimensional images without signal averaging, i.e. imaging at 10 frames per second has been achieved. The three dimensional real-time imaging capability may indeed accelerate clinical observations, reduce motion artefacts and enable important new applications, such as dynamic tracking of hemodynamic and other functional events, circulating cells, etc. Even though for most bio-imaging applications such volumetric imaging rate can be considered sufficient for tracking dynamic events with characteristic time constants down to about a few hundreds of milliseconds, the system can in principle support significantly higher imaging rates, provided the appropriate high repetition pulsed laser technology and data processing capacities become available. Higher frame rate would naturally allow further reducing motion artefacts and enabling tracking of even faster physiological events, e.g. fast heart beat or stimuli. Finally, by imaging at multiple optical wavelengths, the capabilities of the system can be significantly expanded to include the possibility of resolving spectrally-distinct functional markers and dynamic tracking of extrinsically-administered contrast agents. This may e.g. enable high resolution real-time blood oxygenation measurements and improve sensitivity and specificity of pharmacokinetic or targeted molecular imaging studies.

Acknowledgments

The research leading to these results has received funding from the European Union under grant agreement ERC-2010-StG-260991. The authors would also like to thank Dr. J. Gateau for helpful discussion and support during the experiments.